ACS NANO

www.acsnano.org

ARTICLE

# Perfluoroalkyl-Functionalized Graphene Oxide as a Multifunctional Additive for Promoting the Energetic Performance of Aluminum

Yue Jiang, Haiyang Wang, Jihyun Baek, Dongwon Ka, Andy Huu Huynh, Yujie Wang, Michael R. Zachariah, and Xiaolin Zheng*

Cite This: *ACS Nano* 2022, 16, 14658−14665

Read Online

ACCESS | Metrics & More | Article Recommendations | Supporting Information

**ABSTRACT:** **Aluminum (Al) is a widely used metal fuel for energetic applications ranging from space propulsion and exploration, and materials processing, to power generation for nano- and microdevices due to its high energy density and earth abundance. Recently, the ignition and combustion performance of Al particles were found to be improved by graphene-based additives, such as graphene oxide (GO) and graphene fluoride (GF), as their reactions provide heat to accelerate Al oxidation, gas to reduce particle agglomeration, and fluorine-containing species to remove $Al_2O_3$. However, GF is not only expensive but also hydrophobic with poor mixing compatibility with Al particles. Herein, we report a multifunctional graphene-based additive for Al combustion, i.e., perfluoroalkyl-functionalized graphene oxide (CFGO), which integrates the benefits of GO and GF in one material. We compared the effects of CFGO to GO and GF on the ignition and combustion properties of nAl particles using thermogravimetric analysis, differential scanning calorimetry, temperature-jump ignition), Xe flash ignition, and constant-volume combustion test. These experiments confirm that CFGO generates fluorine-containing species, heat, and gases, which collectively lower the ignition threshold, augment the energy release rate, and reduce the combustion product agglomeration of nanosized Al particles, outperforming both GO and GF as additives. This work shows the great potential of using multifunctionalized graphene as an integrated additive for enhancing the ignition and combustion of metals.**

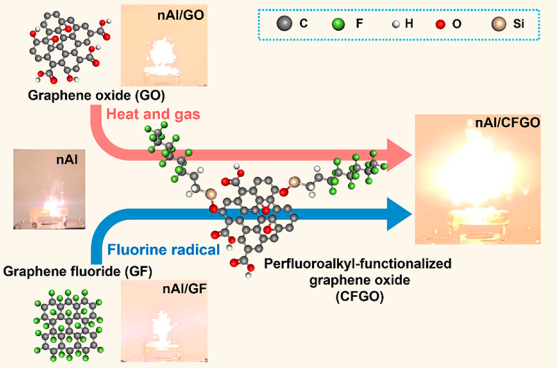


**KEYWORDS:** *energetic materials, aluminum combustion, graphene oxide, graphene fluoride, functionalized grapheme*

Downloaded via UNIV OF CALIFORNIA RIVERSIDE on March 23, 2023 at 17:27:09 (UTC).
See https://pubs.acs.org/sharingguidelines for options on how to legitimately share published articles.

Aluminum (Al), as a metal fuel, has attracted great attention in the past decades due to its high energy density, earth abundance, and low cost as well as its potential in energetic applications, such as power generation, propulsion, and space exploration.[1−5] However, the use of Al particles for energetic application faces several challenges. First, Al particles naturally have a native oxide ($Al_2O_3$) layer (2−5 nm),[6,7] which slows down the mass transport through the oxide layer.[8,9] Second, Al combustion exhibits a size effect. It is well recognized that the nanosized Al (nAl) particles have a higher reactivity and a lower ignition temperature than the micron-sized Al ($\mu$Al) particles.[5,10−12] But nAl particles tend to aggregate, making them burn like the $\mu$Al particles.[13,14] Finally, when Al particles burn, regardless of their sizes, Al particles and their combustion products ($Al_2O_3$) sinter and agglomerate, slowing down the vapor-phase burning of Al and lowering its combustion efficiency.[2,11,15]

Incorporation of additives to Al is an effective approach to address the above-mentioned challenges. Various additives, such as metals (e.g., nickel, titanium),[16−18] metal oxides, (e.g., copper oxide),[19−21] energetic polymers (e.g., metal−organic framework),[22−24] fluoropolymers (e.g., polytetrafluoroethylene (PTFE)),[25−27] metal fluorides (e.g., nickel fluoride),[28] and carbon nanomaterials (e.g., functionalized graphene),[7,29−31] have been reported to promote the ignition and/or combustion of Al by providing at least one of the following benefits. First, some additives release heat through reactions before Al ignition, leading to stressed Al surface and facilitating mass transport of Al and/or O through the native oxide shell.[18] Second, some additives release fluorine-containing species that react with the

Received: May 29, 2022
Accepted: September 9, 2022
Published: September 13, 2022


© 2022 American Chemical Society

https://doi.org/10.1021/acsnano.2c05271
*ACS Nano* 2022, 16, 14658−14665

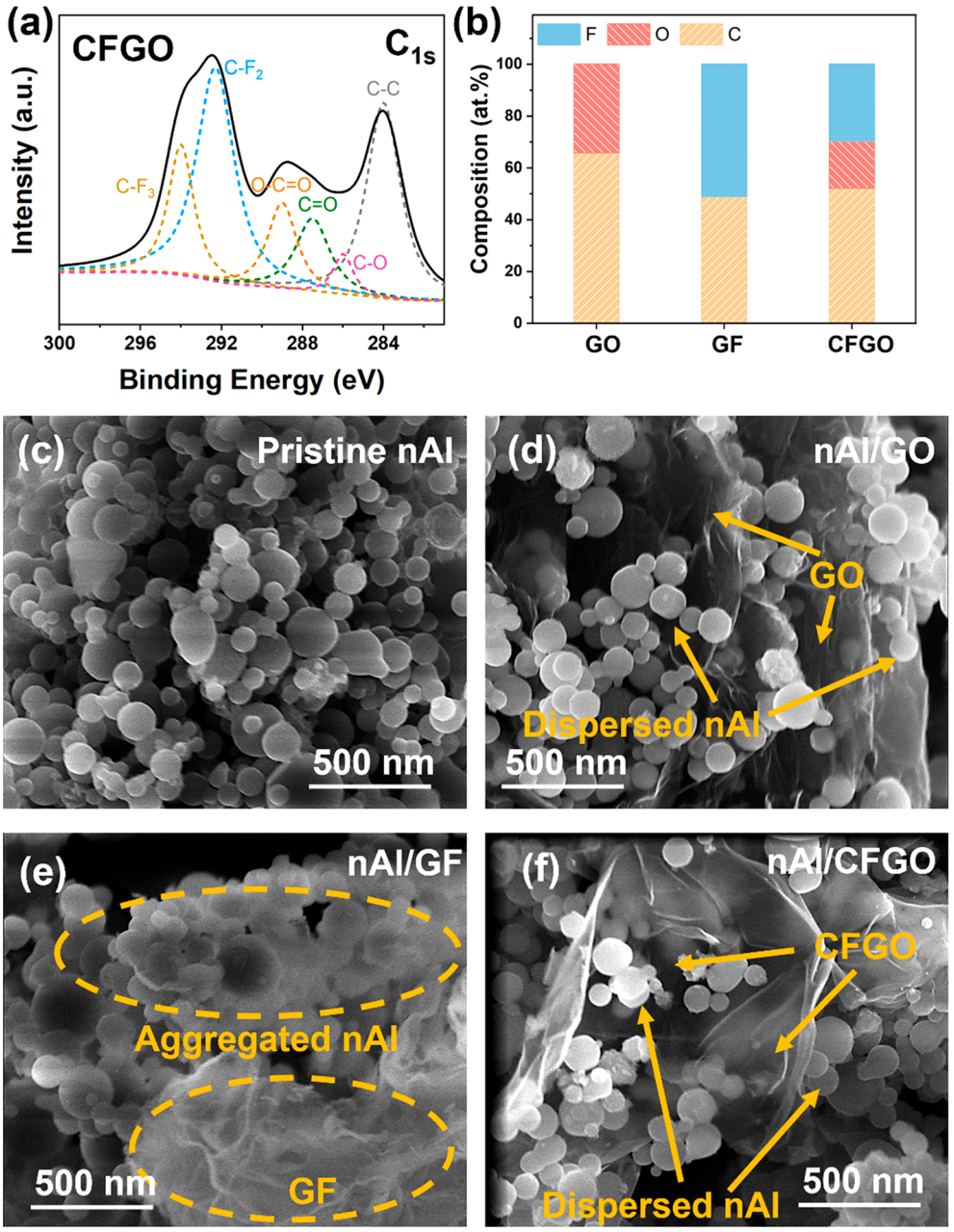


**Figure 1.** (a) XPS spectrum of C 1s of CFGO; (b) elemental composition of C, O, and F in GO, GF, and CFGO; scanning electron microscopy (SEM) images of the (c) pristine nAl; (d) nAl/GO; (e) nAl/GF; (f) nAl/CFGO.

native $Al_2O_3$ shell and/or newly formed $Al_2O_3$, exposing more active Al for oxidation and leading to faster and more complete combustion.[32−34] Finally, some additives, such as metal−organic framework and nitrocellulose, release gaseous products before Al ignition or during Al combustion, which help to break up the aggregates of metal particles or condensed-phase combustion products.[35−37]

Previously, we have investigated the enhancing effects of functionalized graphene additives, including graphene oxide (GO) and graphene fluoride (GF), on the ignition and combustion performance of $\mu$Al particles in the air.[7,38] We found that GO releases heat and gases through a disproportionation reaction at ~200 °C, which initiates the ignition of $\mu$Al and reduces the agglomeration of the combustion products.[38] GF provides fluorocarbon radicals that react with $Al_2O_3$ to form volatile products ($AlF_3$), enhancing the combustion efficiency of $\mu$Al.[7] Moreover, the mixture of GO and GF provides heat, gases, and fluorine-containing species, all of which are desirable for Al combustion. However, GF is hydrophobic and has poor mixing compatibility with GO and Al particles, and GF is of high cost due to its complicated and toxic synthesis approaches.[39,40]

Herein, we report a multifunctional graphene-based additive for Al combustion, perfluoroalkyl-functionalized graphene oxide (CFGO), which integrates the benefits of GO and GF in one material. We compared the effects of CFGO to GO and GF on the ignition and combustion properties of nAl particles using thermogravimetric analysis (TGA), differential scanning calorimetry (DSC), temperature-jump ignition (T-Jump ignition), time-of-flight mass spectrometry (TOFMS), xenon (Xe) flash ignition, and the constant-volume combustion test. These experiments confirm that CFGO generates fluorine-containing species, heat, and gas that lower the ignition threshold, increase


https://doi.org/10.1021/acsnano.2c05271
ACS Nano 2022, 16, 14658−14665

the energy release rate, and reduce the combustion product agglomeration of nAl, outperforming both GO and GF as additives.

## RESULTS AND DISCUSSION

**Material Characterization of CFGO and nAl/CFGO.** The X-ray photoelectron spectroscopy (XPS) spectrum of CFGO in Figure 1a shows that its C 1s peak contains both oxygen (hydroxyl (C−O), carboxylic (O−C═O), and epoxy) and fluorine (fluorocarbon) functional groups, suggesting the successful functionalization of GO with fluorocarbon groups. Further analysis of the XPS data shows that GO has ∼33 atom % of O and GF has ∼50 atom % of F. For comparison, CFGO has O and F content of ∼18 and ∼29 atom %, respectively (Figure 1b). Figure 1c−f shows the morphology of the pristine nAl and nAl/additive (20 wt %) mixtures. The pristine nAl particles are spherical and aggregated (Figure 1c). The nAl particles are less aggregated in the presence of GO (Figure 1d). It has been reported that GO is negatively charged due to the presence of oxygen functional groups and Al particles are positively charged in solution,[41] so Al particles are attracted to the surface of GO and trapped between flakes, which reduces the nAl particle aggregates. In contrast, nAl and GF have opposite hydrophobicity. It has been reported that Al usually has a contact angle below 60° while the contact angle of GF is larger than 135°.[42−44] The hydrophilic nAl and hydrophobic GF do not mix well and agglomerate to themselves (Figure 1e and Figure S2). CFGO, somewhere in between GO and GF, mixes better with nAl particles than GF, with smaller Al aggregates distributed around CFGO (Figure 1f and Figure S2).

**Thermochemical Behaviors of nAl/CFGO under Slow and Fast Heating Conditions.** The thermochemical behaviors of nAl/CFGO and other control groups (nAl/GO, nAl/GF, and nAl) under slow heating conditions were then examined by TGA/DSC. All of the samples were heated from 100 to 700 °C with a heating rate of 10 °C/min, and the results are summarized in Figure 2. The heating stops at 700 °C, right after the melting of Al (660 °C), so that we can focus on the interactions between nAl and additives when Al is in the solid phase. The initial mass drop beginning at 100 °C for all of the samples is attributed to the desorption of water molecules. Around 200−260 °C (Figure 2, region i), only nAl/GO and nAl/CFGO exhibit a mass drop that corresponds to the disproportionation reaction of GO, for which some of the $sp^3$ carbon is oxidized to gases (e.g., $CO_2$) (Figure S1) and others are reduced to $sp^2$ carbon.[45] At 400−500 °C (Figure 2, region ii), both nAl/CFGO and nAl/GF samples exhibit a tiny exothermic peak with a slight mass drop. The TGA-IR analysis of CFGO reveals that $CF_x$ species are produced in this temperature range (Figure S1), so the exothermic peak is attributed to the preignition reactions (PIR)[32] between fluorocarbons and the native $Al_2O_3$ shell. At 500−650 °C (Figure 2, region iii), all samples show an apparent exothermic peak with corresponding mass gains, which is due to the oxidation of Al. In regions ii and iii, the nAl/GO shows a gradual mass drop, which is attributed to the oxidization of carbon to $CO_2$. At 660 °C (Figure 2, region iv), all four samples exhibit a tiny endothermic peak due to the melting of Al, suggesting that the Al is not fully oxidized at this temperature. The TGA/DSC results show that nAl/CFGO has both the disproportionation reaction of GO and preignition reaction between nAl and GF.

To further understand the impact of CFGO on the ignition of nAl, the ignition temperatures of these four samples (nAl, nAl/GO, nAl/GF, and nAl/CFGO) were investigated by a T-jump

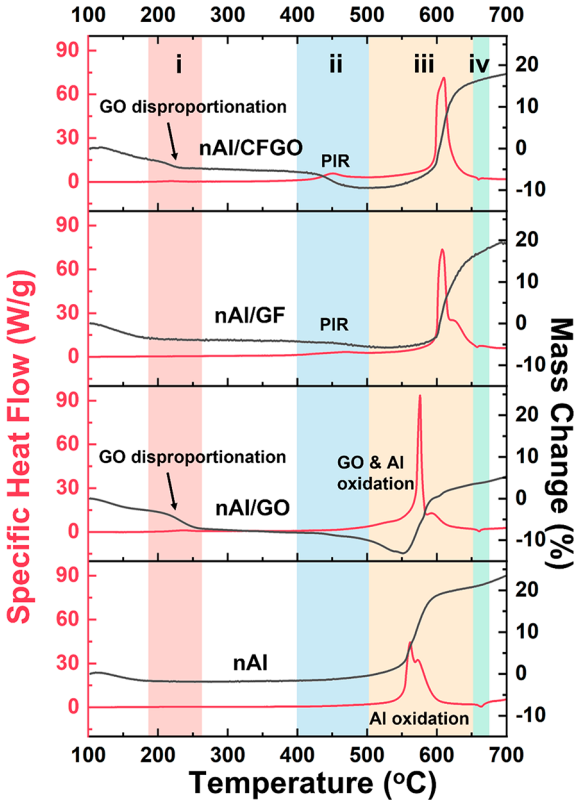


**Figure 2. Investigation of the thermochemical behaviors of nAl with functionalized graphene additives at a slow heating rate (10 °C/min) in air. DSC (red curves, left *y*-axis) and TGA (black curves, right *y*-axis) of pristine nAl, nAl/GO, nAl/GF, and nAl/CFGO composite powders.**

experiment in air. As shown in Figure 3a, pristine nAl particles cannot be ignited by the Pt wire and only sinter slightly. The three nAl samples with additives can be ignited, and the ignition temperature is ∼960 °C for nAl/GO and slightly below 600 °C for both nAl/GF and nAl/CFGO, which implies that F is effective in reducing the ignition threshold of nAl particles through PIR. The insets in Figure 3a also show that nAl/GF and nAl/CFGO burn more vigorously than nAl/GO. Next, the T-jump experiments coupled with mass spectroscopy (MS) were conducted in a vacuum to focus on reactions of the functionalized graphene additives and their interactions with nAl (Figure 3b−d) upon rapid heating. The nAl/GO sample produces $CO_2$ from the disproportionation reaction of GO (Figure 3b). The nAl/GF sample produces AlF from the preignition reaction between fluorocarbons and the oxide on the nAl surface. Moreover, nAl/CFGO produces both $CO_2$ and AlF.

The above results from TGA/DSC, T-jump, and MS indicate that CFGO exhibits characteristics of both GO and GF by releasing heat and gases (mainly $CO_2$) and fluorine-containing species for preignition reaction. Both features facilitate the ignition of nAl. These findings motivate us to further evaluate the effect of CFGO on the combustion of nAl particles.

**Combustion of nAl/CFGO Composite Powders under Fast Heating Conditions.** The combustion performance of these four samples (nAl/CFGO, nAl/GO, nAl/GF, and nAl) was studied in a constant volume vessel, and their reaction was triggered optically by Xe flash. The minimum flash ignition energy was determined by gradually increasing the power of the Xe flash until the sample was ignited.[46,47] The pressure history


https://doi.org/10.1021/acsnano.2c05271
ACS Nano 2022, 16, 14658−14665

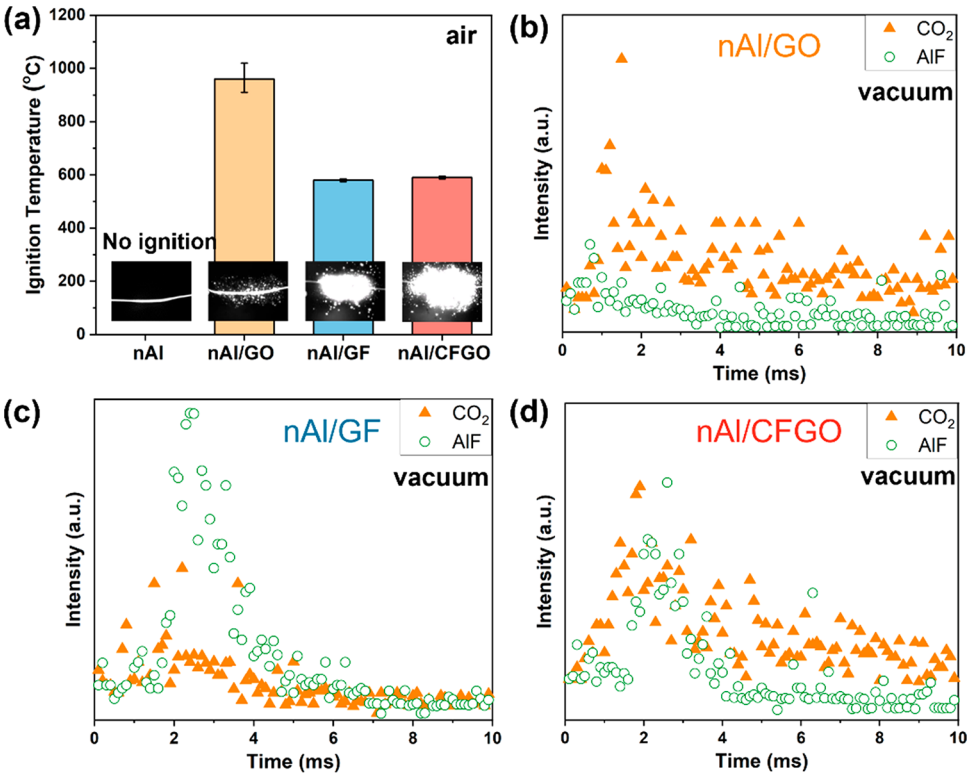


**Figure 3. Characterization of the ignition temperature and species emission in T-jump ignition experiments: (a) ignition temperature of pristine nAl, nAl/GO, nAl/GF, and nAl/CFGO determined by T-jump ignition in 1 atm air. The inserted snapshots represent the largest footprint of the burning of each sample during the T-jump experiment. Time-resolved $CO_2$ and AlF emission of (b) nAl/GO; (c) nAl/GF; and (d) nAl/CFGO measured by T-jump experiment with mass spectroscopy in a vacuum.**

was recorded by a pressure transducer. Figure 4a shows images captured by a high-speed camera and a high-speed infrared (IR) camera. The time-resolved temperature evolution is also extracted from the IR camera videos and plotted in Figure S3. As shown in Figure 4a and Figure S3, nAl/CFGO exhibits the most violent burning and the highest combustion temperature. For nAl/CFGO, the supplementary video shows that burning particles are ejected with smoke generation. Some burning particles exhibit a microexplosion phenomenon (Figure S4), which was observed previously with laser-ignited Al particles.[18] The minimum ignition energy increases in the order of nAl/GF, nAl/CFGO, nAl/GO, and nAl (Figure 4b), implying that the F plays the dominant role in reducing the ignition threshold of nAl while the peak pressure decreases in the order of nAl/CFGO, nAl/GO, nAl/GF, and nAl (Figure 4b). Together, nAl/CFGO exhibits relatively low ignition energy and the highest and fastest pressure rise among all the samples (Figure 4b). With 20 wt % of CFGO, the peak pressure and pressurization rate of flash-ignited nAl particles are increased by over 7- and 6-fold compared to pristine Al particles, respectively. Moreover, we found that the addition of CFGO is more effective than the mixture of GO and GF (Figure S5).

On a separate note, the degree of functionalization of CFGO is tunable, and the synthesis and combustion performance of CFGO with lower and higher degrees of functionalization are shown in the Supporting Information (Figure S6). Based on the oxygen and fluorine contents of all of the functionalized graphene additives investigated (GO, GF, and CFGO with different degrees of functionalization), we also plotted the relationships between the energetic performance and O and F contents as shown in Figure S7. Although there is only a small set of data points, we hope it can serve as a preliminary reference for the design of compositions of multifunctionalized graphene additives for metal combustion. We anticipate more efforts with computational approaches can be done in the future.

The combustion products from the combustion tests (Figure 4a) were evaluated by SEM (Figure 4c–f) and X-ray diffraction (XRD) (Figure 4g). Pristine nAl particles mainly sinter with limited oxidation (Figure 4g), as the morphology of their combustion products (Figure 4c) is similar to that of the pristine nAl before ignition (Figure 1c). The products of nAl/GO contain porous $Al_2O_3$ nanoparticles, which are even smaller than the unreacted nAl particles (Figure 4d), suggesting a large amount of gas generation due to the existence of GO. The products of nAl/GF have relatively larger particles with highly crystallized facets (Figure 4e). These particles contain both $Al_2O_3$ and $AlF_3$ (Figure 4g) and are sintered together while maintaining a porous structure. It should be noted that both nAl/GO and nAl/GF have a relatively low extent of Al oxidation as the XRD of products reveals the dominant existence of metallic Al (Figure 4g). Finally, combustion products of nAl/CFGO (Figure 4f) consist of both partially sintered crystallized particles, similar to that of nAl/GF, and smaller and porous nanoparticles, similar to that of nAl/GO. Interestingly, the products of nAl/CFGO also contain nanowires, as circled in Figure 4f. Those Al and/or $Al_2O_3$ nanowires are likely formed due to the thermal stress accumulation of Al particles confined by graphene nanosheets at high temperatures, according to previous literature.[48] Besides, the nAl/CFGO products also exhibit relatively higher intensities for $\alpha$-$Al_2O_3$ and $\gamma$-$Al_2O_3$ (Figure 4g), which suggests a higher extent of oxidation. $AlF_3$ is also detected in the nAl/CFGO products (Figure 4g),


https://doi.org/10.1021/acsnano.2c05271
ACS Nano 2022, 16, 14658−14665

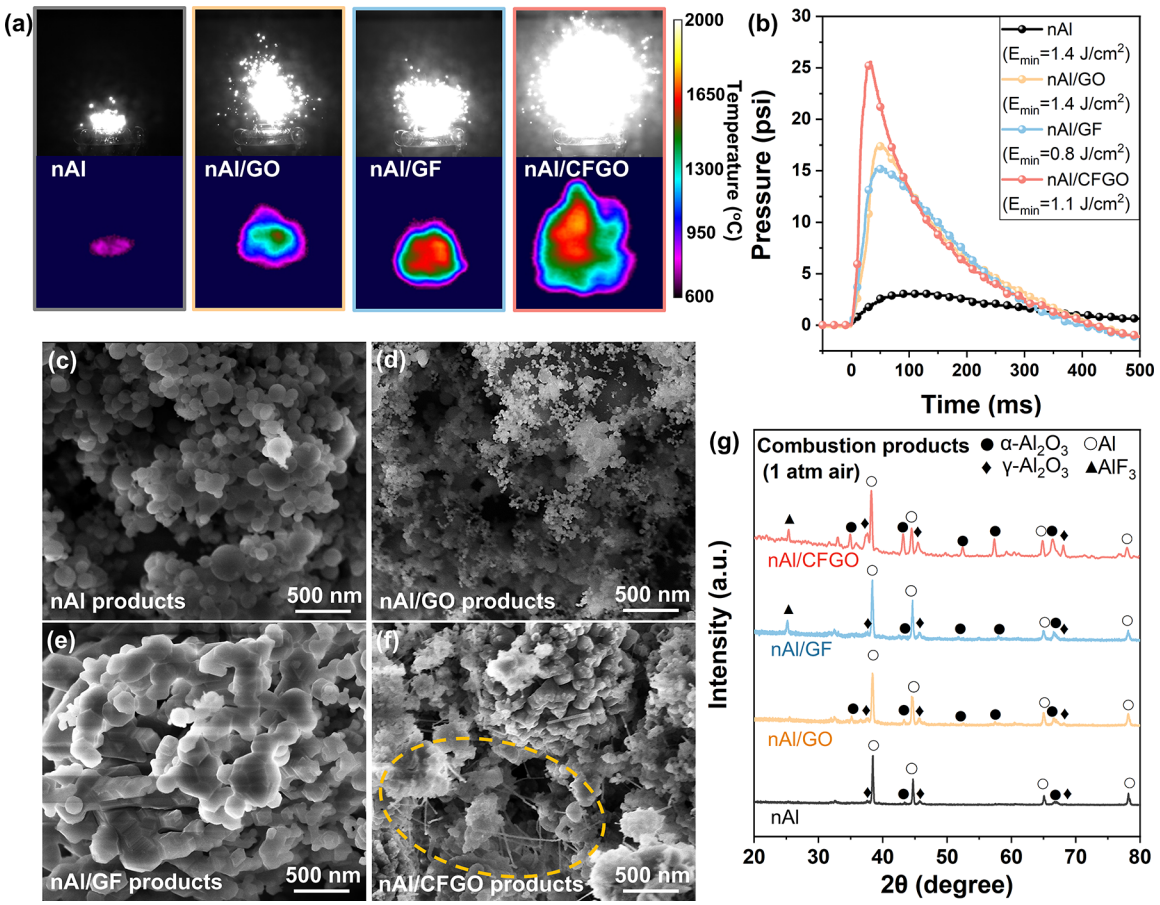


**Figure 4.** (a) Investigation of the burning behaviors and combustion temperature of pristine nAl, nAl/GO, nAl/GF, and nAl/CFGO. All of the samples were ignited by Xe flash (power: 2.1 J/cm$^2$, heating rate: $10^5$–$10^6$ °C/s) in the air. Snapshots were obtained from videos taken by a high-speed camera (black and white) and high-speed IR camera (colorful). (b) Time-resolved pressure evolution of pristine nAl, nAl/GO, nAl/GF, and nAl/CFGO in a constant-volume vessel. All of the samples were ignited by Xe flash (power: 2.1 J/cm$^2$, heating rate: $10^5$–$10^6$ °C/s) in the air. The minimum flash ignition energy ($E_{min}$) of each sample is shown in the legend. (c–g) Combustion products analysis. SEM images of the combustion products of (c) pristine nAl; (d) nAl/GO; (e) nAl/GF; (f) nAl/CFGO; and (g) XRD spectra of the combustion products.

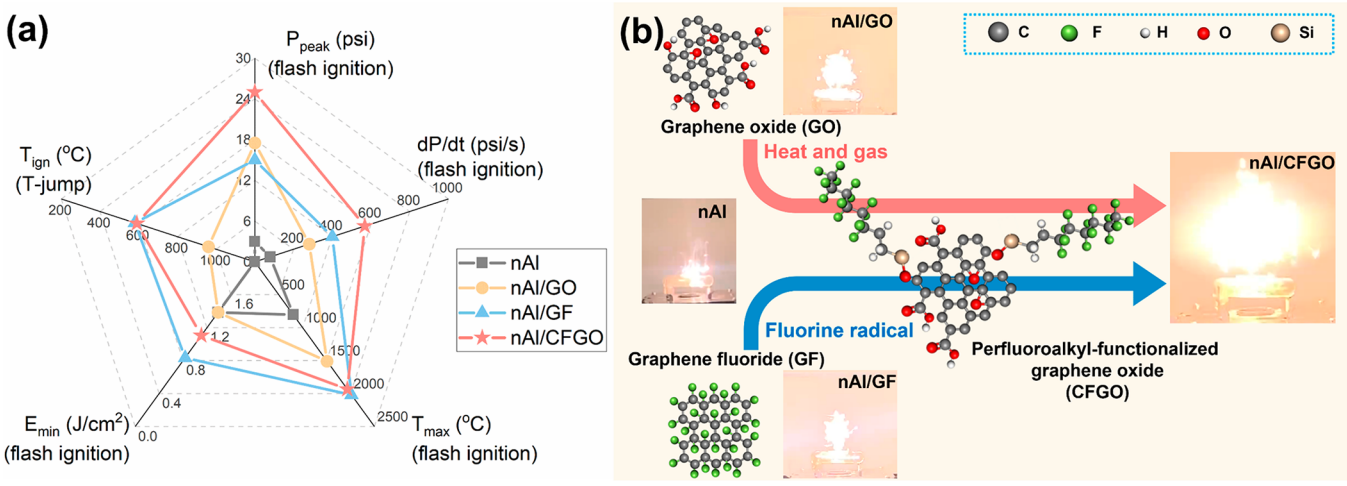


**Figure 5.** (a) Summary of the energetic performance of nAl with various functionalized graphene additives ($T_{ign}$: ignition temperature in T-jump; $E_{min}$: the minimum ignition energy of flash ignition; $T_{max}$: the maximum combustion temperature achieved during the burning of flash-ignited samples in the air; $P_{peak}$: the maximum pressure rises of the flash-ignited samples in a constant-volume vessel; d$P$/d$t$: the pressurization rate of the flash-ignited samples). (b) Schematic summary of this work, showing the molecular structure of different additives, their effects on nAl combustion, and the burning phenomena of nAl with functionalized graphene additives.

confirming the involvement of F during the nAl/CFGO combustion.

All of the aforementioned experimental results are summarized in a spiderweb plot in Figure 5a. nAl/CFGO stands out



https://doi.org/10.1021/acsnano.2c05271
ACS Nano 2022, 16, 14658–14665

among all the samples for its lower ignition threshold and higher combustion temperature and pressure generation. As schematically summarized in Figure 5b, CFGO is GO functionalized with fluorocarbon chains while maintaining some of the oxygen functional groups of GO. By combining oxygen and fluorine functional groups, CFGO could break up the nAl aggregates before combustion, provide heat and fluorine-containing radicals to facilitate the ignition and combustion, and release gaseous products to reduce the agglomeration of combustion products, which collectively lower the ignition threshold and augment the energy release rate of nAl, leading to superior ignition and combustion performance of nAl/CFGO to pristine nAl, nAl/GO, and nAl/GF. All these confirm that CFGO is an effective multifunctional additive for Al combustion.

## CONCLUSIONS

We have demonstrated the use of CFGO as a multifunctional additive to promote the ignition and combustion of Al particles in the air. By comparing the thermochemical behaviors, ignition, and combustion performance of nAl with the addition of GO, GF, and CFGO, we found that CFGO exhibits the beneficial properties of both GO and GF. The presence of fluorine functional groups in CFGO induces the PIR that removes $Al_2O_3$. The oxygen functional groups in CFGO improve mixing with nAl particles and provide heat and gas, which accelerate oxidation and reduce the agglomeration of condensed-phase combustion products. Our work illustrates the potential of multifunctionalized graphene materials as effective additives for metal combustion and will inspire efforts to incorporate more functionalities into this graphene-based system to realize one integrated additive for metal fuels and energetic materials.

## METHODS

**Materials Preparation.** CFGO with both oxygen and fluorine functional groups was synthesized by functionalizing GO (0.5−5 $\mu$m in diameter, 0.8−1.2 nm in thickness, XFNANO) with 1*H*,1*H*,2*H*,2*H*-perfluorooctyltriethoxysilane ($C_{14}H_{19}F_{13}O_3Si$, 98%, Sigma-Aldrich). The degree of fluorocarbon functionalization can be tuned by varying the synthesis conditions, the details of which can be found in the Supporting Information. Specifically, for the CFGO investigated in this work, 20 mg of GO was dispersed in 20 mL of ethanol and sonicated for 1 h. Then, 0.05 mL of 1*H*,1*H*,2*H*,2*H*-perfluorooctyltriethoxysilane was added dropwise into the GO solution, and the suspension was vigorously stirred for 24 h at 65 °C. Afterward, the CFGO was collected four times by centrifuge, and the residual unbound perfluoroalkyl molecules were removed by washing with ethanol after each centrifuge. The collected CFGO powders were dried in a vacuum desiccator for 12 h. To prepare the nAl/CFGO (80/20 wt %) composite powders, 20 mg of CFGO was redispersed in 10 mL of ethanol/deionized water mixture (80/20 v/v) and sonicated for 2 h. Meanwhile, 80 mg of nAl particles (nominal diameter of 70 nm, US Nano, ∼72.5 wt % of active content) were dispersed in 10 mL of ethanol and sonicated for 30 min. Then the two suspensions were mixed and sonicated for 1 h. The mixture powders were collected by filtration and dried in a vacuum desiccator for 12 h. The same method was also used to prepare nAl (80 wt %) mixtures with GO and GF (0.4−5 $\mu$m in diameter, 0.8 nm in thickness, XFNANO).

**Materials Characterization.** The morphologies and elemental compositions of the pristine nAl powders and the nAl/CFGO, nAl/GO, and nAl/GF powders and their combustion products were characterized by SEM (FEI Magellan 400) with energy-dispersive X-ray spectroscopy (EDXS). The bonding and chemical composition of the CFGO were investigated via XPS (PHI VersaProbe) with the CasaXPS software. The phases and compositions of the solid combustion products were characterized by XRD (PANalytical Empyrean).

**TGA/DSC and TGA-IR Measurements.** The thermochemical behaviors of the nAl powders with and without additives were investigated by simultaneous TGA/DSC (Setaram Labsys Evo). For each measurement, 5 mg of the sample powders was placed in a 100 $\mu$L alumina crucible and then heated at a rate of 10 °C/min from 100 to 700 °C in an airflow (40 sccm). After being cooled to room temperature, the sample was reheated with the same setting, and the reheating curve was used to correct the baseline of the first heating process. The gaseous products from CFGO, GO, and GF heated in the air were also analyzed via the TGA-IR mode of Fourier-transform infrared spectroscopy (Nicolet iS50 FTIR Spectrometer, Thermo-Fisher).

**T-Jump/TOFMS Experiments.** Ignition properties of the nAl powders with and without additives were analyzed with T-Jump ignition, a technique described in detail in previous work.[49] The ignition tests were conducted under 1 atm of air. For a typical measurement, the sample powder was dispersed in hexane and sonicated for 30 min and then coated onto a Pt wire (76 $\mu$m in diameter). The sample-coated Pt wire was inserted into a chamber filled with air and rapidly Joule-heated to ∼1000 °C by a 3 ms pulse at a heating rate of $\sim 10^5$ K/s. The temporal voltage and current of the wire were recorded during heating, and the instantaneous temperature was calculated based on the Callendar-Van Dusen equation. The ignition event on the Pt wire was recorded by a Vision Research Phantom v12.0 high-speed camera. The ignition temperature was estimated by correlating the video and the measured wire temperature based on triple tests, and the average value with standard deviation is reported. The transient gaseous species during the ignition and combustion events were detected by conducting T-jump/TOFMS. The details about T-Jump/TOFMS can be found in our previous studies.[50,51]

**Flash Ignition and Time-Resolved Pressure Measurement.** The ignition and combustion of the nAl/additive samples were investigated by measuring their temperature and pressure rises upon Xe flash ignition at a heating rate of $\sim 10^5$−$10^6$ °C/s. The experimental details have been reported in our previous works.[7,38] For a typical flash ignition experiment, 5 mg of sample powders was placed on a 1 mm thick glass slide on top of a commercial Xe flash ring tube (AlienBees B1600). To minimize the effect of porosity, all sample powders were packed to have a porosity of ∼85% in these experiments. The burning process of flash-ignited samples was recorded by a high-speed camera (Photron FASTCAM SA5) at 5000 fps and a high-speed IR camera (FLIR X6900sc) at 1000 fps. For the time-resolved pressure measurement under constant-volume conditions, 20 mg of powders was loaded in a 20 mL glass vial with air, and the vial was then placed on top of the Xe flash ring tube and then ignited at a power of 2.1 J/cm$^2$. The pressure generation from nAl combustion was recorded by a pressure transducer (603B1, Kistler, Inc.). The temperature of the burning particles was measured by the IR camera at 1000 fps, and we used the maximum temperature in each frame to plot the temperature vs time profiles. For each sample, the temperature measurement was repeated three times to obtain the error bars. The maximum temperature throughout the entire period was defined as $T_{max}$.

## ASSOCIATED CONTENT

### Supporting Information

The Supporting Information is available free of charge at https://pubs.acs.org/doi/10.1021/acsnano.2c05271.

TGA-IR results of CFGO, GO, and GF (Figure S1); SEM/EDXS of nAl/GO, nAl/GF, and nAl/CFGO mixtures (Figure S2); temperature history during the combustion of nAl, nAl/GO, nAl/GF, and nAl/CFGO samples (Figure S3); sequential burning snapshots of nAl/CFGO composite powders triggered by Xe flash ignition in air (Figure S4); time-resolved pressure evolution of nAl/GO-GF sample compared with nAl, nAl/GO, nAl/GF, and nAl/CFGO (Figure S5); tunability of the functionalization degree of CFGO and the effect of functionalization degree on the combustion



https://doi.org/10.1021/acsnano.2c05271
ACS Nano 2022, 16, 14658−14665

performance of nAl/CFGO (Figure S6); relationships between energetic performance and fluorine and oxygen contents (Figure S7) (PDF)

Burning process of nAl/CFGO sample triggered by Xe flash ignition in air (MP4)

## AUTHOR INFORMATION


### Corresponding Author

**Xiaolin Zheng** − *Department of Mechanical Engineering, Stanford University, Stanford, California 94305, United States;* orcid.org/0000-0002-8889-7873; Email: xlzheng@stanford.edu

### Authors

**Yue Jiang** − *Department of Mechanical Engineering, Stanford University, Stanford, California 94305, United States;* orcid.org/0000-0002-6017-8551

**Haiyang Wang** − *Department of Chemical and Environmental Engineering, University of California, Riverside, California 92521, United States;* orcid.org/0000-0001-5200-3965

**Jihyun Baek** − *Department of Mechanical Engineering, Stanford University, Stanford, California 94305, United States;* orcid.org/0000-0002-1917-759X

**Dongwon Ka** − *Department of Mechanical Engineering, Stanford University, Stanford, California 94305, United States*

**Andy Huu Huynh** − *Department of Mechanical Engineering, Stanford University, Stanford, California 94305, United States*

**Yujie Wang** − *Department of Chemical and Environmental Engineering, University of California, Riverside, California 92521, United States*

**Michael R. Zachariah** − *Department of Chemical and Environmental Engineering, University of California, Riverside, California 92521, United States;* orcid.org/0000-0002-4115-3324

Complete contact information is available at: https://pubs.acs.org/10.1021/acsnano.2c05271


### Notes

The authors declare no competing financial interest.

## ACKNOWLEDGMENTS

This work was supported by the Office of Naval Research managed by Chad Stoltz under Agreement No. N00014-19-1-2085. University of California authors were supported by the Office of Naval Research.

## REFERENCES


(1) Yetter, R. A. Progress Towards Nanoengineered Energetic Materials. *Proceedings of the Combustion Institute* **2021**, *38*, 57−81.

(2) Babuk, V.; Dolotkazin, I.; Gamsov, A.; Glebov, A.; DeLuca, L. T.; Galfetti, L. Nanoaluminum as A Solid Propellant Fuel. *Journal of Propulsion and Power* **2009**, *25*, 482−489.

(3) Wang, L. L.; Munir, Z. A.; Maximov, Y. M. Thermite Reactions: Their Utilization in the Synthesis and Processing of Materials. *J. Mater. Sci.* **1993**, *28*, 3693−3708.

(4) Gan, Y.; Qiao, L. Combustion Characteristics of Fuel Droplets with Addition of Nano and Micron-Sized Aluminum Particles. *Combust. Flame* **2011**, *158*, 354−368.

(5) Pang, W.; Li, Y.; DeLuca, L. T.; Liang, D.; Qin, Z.; Liu, X.; Xu, H.; Fan, X. Effect of Metal Nanopowders on the Performance of Solid Rocket Propellants: A Review. *Nanomaterials* **2021**, *11*, 2749.

(6) Yetter, R. A.; Risha, G. A.; Son, S. F. Metal Particle Combustion and Nanotechnology. *Proceedings of the Combustion Institute* **2009**, *32*, 1819−1838.

(7) Jiang, Y.; Deng, S.; Hong, S.; Tiwari, S.; Chen, H.; Nomura, K.-i.; Kalia, R. K.; Nakano, A.; Vashishta, P.; Zachariah, M. R.; Zheng, X. Synergistically Chemical and Thermal Coupling between Graphene Oxide and Graphene Fluoride for Enhancing Aluminum Combustion. *ACS Appl. Mater. Interfaces* **2020**, *12*, 7451−7458.

(8) Wang, W.; Clark, R.; Nakano, A.; Kalia, R. K.; Vashishta, P. Effects of Oxide-Shell Structures on the Dynamics of Oxidation of Al Nanoparticles. *Appl. Phys. Lett.* **2010**, *96*, 181906.

(9) Wang, J.; Qu, Y.; Gong, F.; Shen, J.; Zhang, L. A Promising Strategy to Obtain High Energy Output and Combustion Properties by Self-Activation of Nano-Al. *Combust. Flame* **2019**, *204*, 220−226.

(10) Huang, Y.; Risha, G.; Yang, V.; Yetter, R., Analysis of Nano-Aluminum Particle Dust Cloud Combustion in Different Oxidizer Environments. In *43rd AIAA Aerospace Sciences Meeting and Exhibit*; American Institute of Aeronautics and Astronautics, 2005.

(11) Sundaram, D. S.; Yang, V.; Zarko, V. E. Combustion of Nano Aluminum Particles (Review). *Combustion, Explosion, and Shock Waves* **2015**, *51*, 173−196.

(12) Huang, Y.; Risha, G. A.; Yang, V.; Yetter, R. A. Combustion of Bimodal Nano/Micron-Sized Aluminum Particle Dust in Air. *Proceedings of the Combustion Institute* **2007**, *31*, 2001−2009.

(13) Deng, S.; Jiang, Y.; Huang, S.; Shi, X.; Zhao, J.; Zheng, X. Tuning the Morphological, Ignition and Combustion Properties of Micron-Al/CuO Thermites Through Different Synthesis Approaches. *Combust. Flame* **2018**, *195*, 303−310.

(14) Wei, D.; Dave, R.; Pfeffer, R. Mixing and Characterization of Nanosized Powders: An Assessment of Different Techniques. *J. Nanopart. Res.* **2002**, *4*, 21−41.

(15) Wang, H.; Kline, D. J.; Zachariah, M. R. In-Operando High-Speed Microscopy and Thermometry of Reaction Propagation and Sintering in A Nanocomposite. *Nat. Commun.* **2019**, *10*, 3032.

(16) Zhao, W.; Wang, X.; Wang, H.; Wu, T.; Kline, D. J.; Rehwoldt, M.; Ren, H.; Zachariah, M. R. Titanium Enhanced Ignition and Combustion of Al/$I_2O_5$ Mesoparticle Composites. *Combust. Flame* **2020**, *212*, 245−251.

(17) Sundaram, D. S.; Puri, P.; Yang, V. Thermochemical Behavior of Nickel-Coated Nanoaluminum Particles. *J. Phys. Chem. C* **2013**, *117*, 7858−7869.

(18) Wang, C.; Zou, X.; Yin, S.; Wang, J.; Li, H.; Liu, Y.; Wang, N.; Shi, B. Improvement of Ignition and Combustion Performance of Micro-Aluminum Particles by Double-Shell Nickel-Phosphorus Alloy Coating. *Chemical Engineering Journal* **2022**, *433*, 133585.

(19) Wang, H.; Jian, G.; Egan, G. C.; Zachariah, M. R. Assembly and Reactive Properties of Al/CuO Based Nanothermite Microparticles. *Combust. Flame* **2014**, *161*, 2203−2208.

(20) Hunt, E. M.; Malcolm, S.; Pantoya, M. L.; Davis, F. Impact Ignition of Nano and Micron Composite Energetic Materials. *International Journal of Impact Engineering* **2009**, *36*, 842−846.

(21) Wang, N.; Hu, Y.; Ke, X.; Xiao, L.; Zhou, X.; Peng, S.; Hao, G.; Jiang, W. Enhanced-Absorption Template Method for Preparation of Double-Shell NiO Hollow Nanospheres with Controllable Particle Size for Nanothermite Application. *Chemical Engineering Journal* **2020**, *379*, 122330.

(22) Ma, X.; Zhu, Y.; Cheng, S.; Zheng, H.; Liu, Y.; Qiao, Z.; Yang, G.; Zhang, K. Energetic Composites Based on Nano-Al and Energetic Coordination Polymers (ECPs): The "Father-Son" Effect of ECPs. *Chemical Engineering Journal* **2020**, *392*, 123719.

(23) Xue, K.; Li, H.; Pan, L.; Liu, Y.; Zhang, X.; Zou, J.-J. Bifunctional Core-Shell nAl@MOF Energetic Particles with Enhanced Ignition and Combustion Performance. *Chemical Engineering Journal* **2022**, *430*, 132909.

(24) Su, H.; Zhang, J.; Du, Y.; Zhang, P.; Li, S.; Fang, T.; Pang, S. New Roles of Metal-Organic Frameworks: Fuels for Aluminum-Free Energetic Thermites with Low Ignition Temperatures, High Peak Pressures and High Activity. *Combust. Flame* **2018**, *191*, 32−38.

(25) Sippel, T. R.; Son, S. F.; Groven, L. J. Aluminum Agglomeration Reduction in A Composite Propellant using Tailored Al/PTFE Particles. *Combust. Flame* **2014**, *161*, 311−321.

(26) Huang, S.; Hong, S.; Su, Y.; Jiang, Y.; Fukushima, S.; Gill, T. M.; Yilmaz, N. E. D.; Tiwari, S.; Nomura, K.-i.; Kalia, R. K.; Nakano, A.; Shimojo, F.; Vashishta, P.; Chen, M.; Zheng, X. Enhancing Combustion Performance of Nano-Al/PVDF Composites with β-PVDF. *Combust. Flame* **2020**, *219*, 467−477.
(27) Huang, S.; Pan, M.; Deng, S.; Jiang, Y.; Zhao, J.; Levy-Wendt, B.; Tang, S. K. Y.; Zheng, X. Modified Micro-Emulsion Synthesis of Highly Dispersed Al/PVDF Composites with Enhanced Combustion Properties. *Adv. Eng. Mater.* **2019**, *21*, 1801330.
(28) Valluri, S. K.; Bushiri, D.; Schoenitz, M.; Dreizin, E. Fuel-Rich Aluminum-Nickel Fluoride Reactive Composites. *Combust. Flame* **2019**, *210*, 439−453.
(29) Zhu, B.; Zhang, S.; Sun, Y.; Ji, Y.; Wang, J. Fluorinated Graphene Improving Thermal Reaction and Combustion Characteristics of Nano-Aluminum Powder. *Thermochim. Acta* **2021**, *705*, 179038.
(30) Wang, A.; Bok, S.; Mathai, C. J.; Thiruvengadathan, R.; Darr, C. M.; Chen, H.; Zachariah, M. R.; Gangopadhyay, K.; McFarland, J. A.; Maschmann, M. R. Synthesis, Characterization and Nanoenergetic Utilizations of Fluorine, Oxygen Co-Functionalized Graphene by One-Step $XeF_2$ Exposure. *Combust. Flame* **2020**, *215*, 324−332.
(31) Wang, Y.; Li, F.; Shen, Y.; Wang, C.-a.; Zhang, Z.; Xu, J.; Ye, Y.; Shen, R. Fabrication of High Electrostatic Safety Metastable Al/CuO Nanocomposites Doped with Nitro-Functionalized Graphene with Fast Initiation Ability and Tunable Reaction Performance. *Combust. Flame* **2021**, *233*, 111580.
(32) McCollum, J.; Pantoya, M. L.; Iacono, S. T. Activating Aluminum Reactivity with Fluoropolymer Coatings for Improved Energetic Composite Combustion. *ACS Appl. Mater. Interfaces* **2015**, *7*, 18742−18749.
(33) Ao, W.; Liu, P.; Liu, H.; Wu, S.; Tao, B.; Huang, X.; Li, L. K. B. Tuning the Agglomeration and Combustion Characteristics of Aluminized Propellants via A New Functionalized Fluoropolymer. *Chemical Engineering Journal* **2020**, *382*, 122987.
(34) Jiang, Y.; Wang, Y.; Baek, J.; Wang, H.; Gottfried, J. L.; Wu, C.-C.; Shi, X.; Zachariah, M. R.; Zheng, X. Ignition and Combustion of Perfluoroalkyl-Functionalized Aluminum Nanoparticles and Nano-thermite. *Combust. Flame* **2022**, *242*, 112170.
(35) He, W.; Ao, W.; Yang, G.; Yang, Z.; Guo, Z.; Liu, P.-J.; Yan, Q.-L. Metastable Energetic Nanocomposites of MOF-Activated Aluminum Featured with Multi-Level Energy Releases. *Chemical Engineering Journal* **2020**, *381*, 122623.
(36) Huang, C.; Yang, Z.; Li, Y.; Zheng, B.; Yan, Q.; Guan, L.; Luo, G.; Li, S.; Nie, F. Incorporation of High Explosives into Nano-Aluminum Based Microspheres to Improve Reactivity. *Chemical Engineering Journal* **2020**, *383*, 123110.
(37) Wang, H.; Jian, G.; Yan, S.; DeLisio, J. B.; Huang, C.; Zachariah, M. R. Electrospray Formation of Gelled Nano-Aluminum Microspheres with Superior Reactivity. *ACS Appl. Mater. Interfaces* **2013**, *5*, 6797−6801.
(38) Jiang, Y.; Deng, S.; Hong, S.; Zhao, J.; Huang, S.; Wu, C.-C.; Gottfried, J. L.; Nomura, K.-i.; Li, Y.; Tiwari, S.; Kalia, R. K.; Vashishta, P.; Nakano, A.; Zheng, X. Energetic Performance of Optically Activated Aluminum/Graphene Oxide Composites. *ACS Nano* **2018**, *12*, 11366−11375.
(39) Jiang, Y.; Demko, A. R.; Baek, J.; Shi, X.; Vallez, L.; Ning, R.; Zheng, X. Facilitating Laser Ignition and Combustion of Boron with A Mixture of Graphene Oxide and Graphite Fluoride. *Applications in Energy and Combustion Science* **2020**, *1*−*4*, 100013.
(40) Feng, W.; Long, P.; Feng, Y.; Li, Y. Two-Dimensional Fluorinated Graphene: Synthesis, Structures, Properties and Applications. *Advanced Science* **2016**, *3*, 1500413.
(41) Li, Z.; Fan, G.; Tan, Z.; Guo, Q.; Xiong, D.; Su, Y.; Li, Z.; Zhang, D. Uniform Dispersion of Graphene Oxide in Aluminum Powder by Direct Electrostatic Adsorption for Fabrication of Graphene/Aluminum Composites. *Nanotechnology* **2014**, *25*, 325601.
(42) López, C.; Galmés, B.; Soberats, B.; Frontera, A.; Rotger, C.; Costa, A. Surface Modification of Pseudoboehmite-Coated Aluminum Plates with Squaramic Acid Amphiphiles. *ACS omega* **2019**, *4*, 14868−14874.
(43) Wang, X.; Dai, Y.; Wang, W.; Ren, M.; Li, B.; Fan, C.; Liu, X. Fluorographene with High Fluorine/Carbon Ratio: A Nanofiller for Preparing Low-κ Polyimide Hybrid Films. *ACS Appl. Mater. Interfaces* **2014**, *6*, 16182−16188.
(44) Mazánek, V.; Jankovský, O.; Luxa, J.; Sedmidubský, D.; Janoušek, Z.; Šembera, F.; Mikulics, M.; Sofer, Z. Tuning of Fluorine Content in Graphene: Towards Large-Scale Production of Stoichiometric Fluorographene. *Nanoscale* **2015**, *7*, 13646−13655.
(45) Krishnan, D.; Kim, F.; Luo, J.; Cruz-Silva, R.; Cote, L. J.; Jang, H. D.; Huang, J. Energetic Graphene Oxide: Challenges and Opportunities. *Nano Today* **2012**, *7*, 137−152.
(46) Ohkura, Y.; Weisse, J. M.; Cai, L.; Zheng, X. Flash Ignition of Freestanding Porous Silicon Films: Effects of Film Thickness and Porosity. *Nano Lett.* **2013**, *13*, 5528−5533.
(47) Huang, S.; Parimi, V. S.; Deng, S.; Lingamneni, S.; Zheng, X. Facile Thermal and Optical Ignition of Silicon Nanoparticles and Micron Particles. *Nano Lett.* **2017**, *17*, 5925−5930.
(48) Chen, Y.; Wang, Y.; Zhu, S.; Chen, C.; Danner, V. A.; Li, Y.; Dai, J.; Li, H.; Fu, K. K.; Li, T.; Liu, Y.; Hu, L. One-Step, Catalyst-Free, Scalable in Situ Synthesis of Single-Crystal Aluminum Nanowires in Confined Graphene Space. *ACS Appl. Mater. Interfaces* **2019**, *11*, 6009−6014.
(49) Zhou, W.; DeLisio, J. B.; Wang, X.; Egan, G. C.; Zachariah, M. R. Evaluating Free vs Bound Oxygen on Ignition of Nano-Aluminum Based Energetics Leads to A Critical Reaction Rate Criterion. *J. Appl. Phys.* **2015**, *118*, 114303.
(50) Zhou, L.; Piekiel, N.; Chowdhury, S.; Zachariah, M. R. Time-Resolved Mass Spectrometry of the Exothermic Reaction between Nanoaluminum and Metal Oxides: The Role of Oxygen Release. *J. Phys. Chem. C* **2010**, *114*, 14269−14275.
(51) Jian, G.; Piekiel, N. W.; Zachariah, M. R. Time-Resolved Mass Spectrometry of Nano-Al and Nano-Al/CuO Thermite under Rapid Heating: A Mechanistic Study. *J. Phys. Chem. C* **2012**, *116*, 26881−26887.

## Recommended by ACS

**Application of 2D Materials for Adsorptive Removal of Air Pollutants**
Jun Tae Kim, Sang Ouk Kim, *et al.*
NOVEMBER 10, 2022
ACS NANO
READ

**MIL-101(Fe) Networks Supported on Fluorinated Graphene Nanosheets as Coatings for Oil Sorption**
Yogapriya Ravi, K. K. R. Datta, *et al.*
MARCH 30, 2022
ACS APPLIED NANO MATERIALS
READ

**Bio-Based Aerogel Based on Bamboo, Waste Paper, and Reduced Graphene Oxide for Oil/Water Separation**
Jiwei Huang, Ting Liu, *et al.*
FEBRUARY 23, 2022
LANGMUIR
READ

**Effects of MgO, γ-$Al_2O_3$, and $TiO_2$ Nanoparticles at Low Concentrations on Interfacial Tension (IFT), Rock Wettability, and Oil Recovery by Spontaneous Imbibition...**
Iman Nowrouzi, Amir H. Mohammadi, *et al.*
JUNE 16, 2022
ACS OMEGA
READ

Get More Suggestions >


https://doi.org/10.1021/acsnano.2c05271
*ACS Nano* 2022, 16, 14658−14665